Nanoscale Research Letters

NANO EXPRESS

Strain Engineering on the Electronic and Optical Properties of WSSe Bilayer

Jian Guo, Congming Ke, Yaping Wu[*] and Junyong Kang

Abstract

Controllable optical properties are important for optoelectronic applications. Based on the unique properties and potential applications of two-dimensional Janus WSSe, we systematically investigate the strain-modulated electronic and optical properties of WSSe bilayer through the first-principle calculations. The preferred stacking configurations and chalcogen orders are determined by the binding energies. The bandgap of all the stable structures are found sensitive to the external stress and could be tailored from semiconductor to metallicity under appropriate compressive strains. Atomic orbital projected energy bands reveal a positive correlation between the degeneracy and the structural symmetry, which explains the bandgap evolutions. Dipole transition preference is tuned by the biaxial strain. A controllable transformation between anisotropic and isotropic optical properties is achieved under an around − 6%~− 4% critical strain. The strain controllable electronic and optical properties of the WSSe bilayer may open up an important path for exploring next-generation optoelectronic applications.

Keywords: WSSe bilayer, Biaxial strain, Optical anisotropy, The first-principle calculations

Introduction

Two-dimensional (2D) materials with their novel properties have been showing great application prospect in next-generation electronic devices. As a promising candidate, 2D-layered transition metal dichalcogenides (TMDCs) with tunable bandgap were widely studied over the past decade and were intensively exploited as tunneling field-effect transistors [1], light-emitting diodes, photodetectors [2, 3], sensors [4], and so on.

Beyond the highly symmetrical MX_2 (M = Mo, W; X = S, Se, Te) configuration, new Janus structural TMDCs, with the chemical formula of MXY (M = Mo, W; $X \neq Y$ = S, Se, Te) have attracted increasing interest due to their distinctive optical and electronic properties. The monolayer MXY is constructed by two different chalcogen atom layers marked as A, A' and one transition-metal atom layer B to form an ABA' atomic stacking. Compared with that of MX_2, MXY possesses an asymmetry-ordered configuration with the breaking of

mirror symmetry, which leads to a vertical dipole and enhanced Rashba spin-orbit coupling [5]. Geometric and electronic structures of Janus WSSe have already been reported and proved to have plenty of distinguishing features different from both WS_2 and WSe_2. For instance, the hydrogen evolution reaction catalytic activity of WSSe was found superior to that of current TMD-based catalysts [6]. The WSSe field-effect transistors also have achieved better performance in electron mobilities and I_{ON}/I_{OFF} ratio than that of conventional TMD monolayers [7]. Despite the exciting characters of the intrinsic monolayer, Janus TMDCs with bilayer and multilayer thickness and various stacking structures may possess profound physical connotations considering the asymmetry of the MXY configuration. For example, the Se-S-Se-S-ordered WSSe bilayer was predicted to improve the efficiency of photoelectric conversion efficiency for solar cell applications [8].

Based on the unique Janus TMDC materials, realizing an accurate control of their electronic and optical properties is vital to meeting the multiple needs of device design. Electric field [9, 10], strain [11, 12], surface decoration [13, 14], and magnetic doping [15–17] have

* Correspondence: ypwu@xmu.edu.cn
Department of Physics, OSED, Fujian Provincial Key Laboratory of Semiconductor Materials and Applications, Jiujiang Research Insititute, Xiamen University, Xiamen 361005, People's Republic of China

Guo *et al. Nanoscale Research Letters*   (2020) 15:97

Page 2 of 9

been proven as effective means to modulate the electronic and optical behaviors of 2D TMDCs. Among these methods, strain engineering is reversible with the controllable process, while without generating additional lattice defects and damage in the materials. Besides, strain engineering will alter the structural symmetry, which may give rise to the polarized characteristics of 2D materials and endow them with great prospects in future applications. As has been reported, the strained WSe_2 monolayers show obvious variation in electronic band structure [18–22] and demonstrate unique advantages in the applications of photoactive devices [23], valleytronics [18, 24], photodetectors [25], and anode material for Li-ion battery [26]. Nevertheless, strain engineering on the electronic and optical properties, such as band evolution and optical anisotropy of 2D Janus WSSe bilayer has not yet been reported so far.

In this work, we perform an investigation on the strain modulation of the electronic and optical properties of WSSe bilayer through the first-principle density function calculations. The investigation is initiated with the determination of the most favorable stacking order of the bilayer. Strain-dependent band structures of the three stable configurations are calculated. The bandgaps of

WSSe bilayers are tailored and the atomic orbital contribution is revealed to understand the related mechanism. Optical anisotropy is also modulated by tuning the dielectric properties through the applied strain. A controllable transformation between anisotropic and isotropic optical properties is demonstrated.

Computational Method

All theoretical calculations are based on the density functional theory (DFT) with the generalized gradient approximation (GGA). The accurate projector-augmented wave (PAW) method, as implemented in the Vienna *Ab-initio* Simulation Package (VASP) [27–29] code is used. A slab model with a 1×1 unit cell is constructed, and a 20 Å vacuum layer along the z direction is used to minimize artificial interactions between neighboring slabs. The valence electron configurations of W, S, and Se atoms adopted are $5p^6 5d^4 6s^2$, $2s^2 3p^4$, and $4s^2 4p^4$, respectively. The GGA [30] with Perdew-Burke-Ernzerhof (PBE) [31] parameterization is employed as the exchange-correlation functional. Electron wave functions are expanded in plane waves with an energy cutoff of 400 eV. The Brillouin zone is sampled with a $19 \times 19 \times 1$ Monkhorst-Pack grid of k points. The DFT-D2
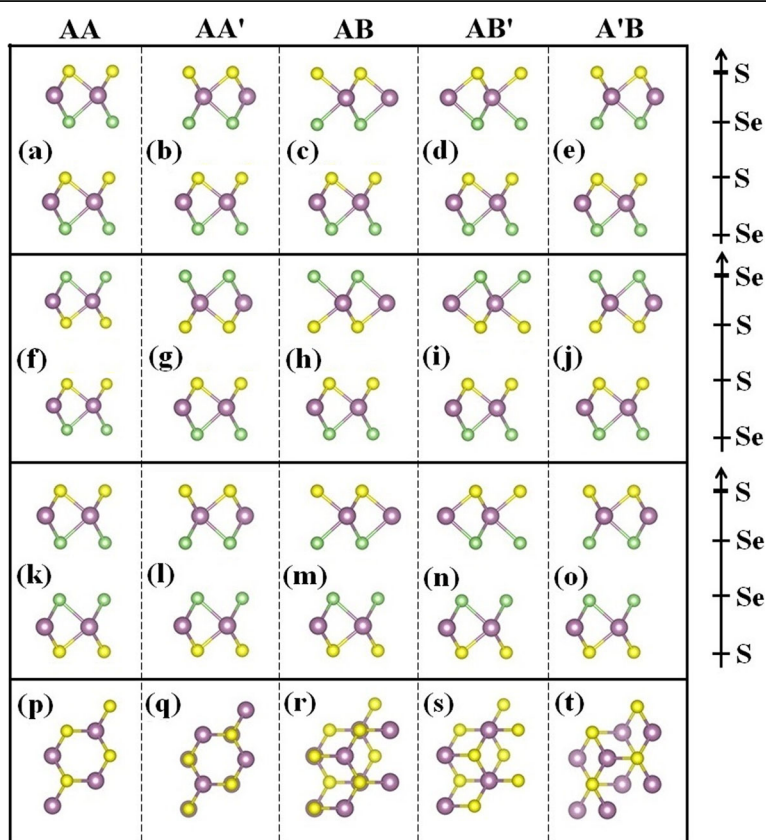

Fig. 1 Top and side views of the atomic configuration of WSSe bilayer. The purple balls represent the W atoms, and the yellow and green balls represent the S and Se atoms, respectively
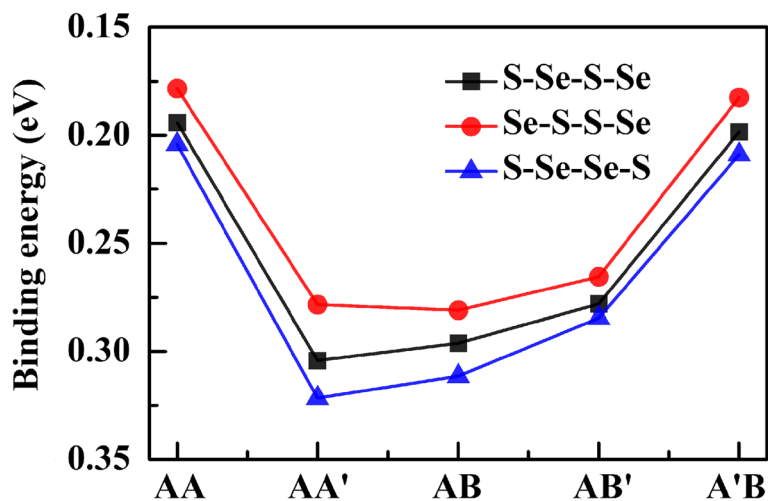
Fig. 2 Binding energies of all the equilibrium geometric configurations of WSSe bilayer

dispersion correction method is included in the structural relaxation and electronic structure calculations to correctly describe the effect of van der Waals integrations. All atomic degrees of freedom, including lattice constants, are fully relaxed with self-consistent convergence criteria of 0.01 eV/Å and 10^{-6} eV for the atomic forces and total energy, respectively.

Results and Discussion

The Janus WSSe monolayer has a hexagonal lattice, where the unit cell consists of a middle W atom in its planar honeycomb lattice that bonded three-coordinately with the surface S and Se atoms. The optimized lattice constant of WSSe is 3.23 Å with the W-S and W-Se bond lengths of 2.42 and 2.53 Å, respectively, which are aligned with the previous reported values [32]. According to the

structural symmetry, five different stacking configurations of WSSe bilayer are taken into account, which is marked as AA, AA', AB, AB', and A'B, respectively. For each stacking, three different orders of chalcogen layers: S-Se-S-Se, Se-S-S-Se, and S-Se-Se-S are considered. All equilibrium geometric configurations of the WSSe bilayer are depicted in Fig. 1. Each configuration is fully relaxed respectively to optimize the interlayer spacing.

In order to determine the structural stability of the WSSe bilayer quantitatively, the binding energies E_b of all above geometric configurations are calculated from the relation:

$$E_b = 2E_{WSSe} - E_{bilayer,}$$

where $E_{bilayer}$ and E_{WSSe} are the total energies of WSSe bilayer and monolayer, respectively.
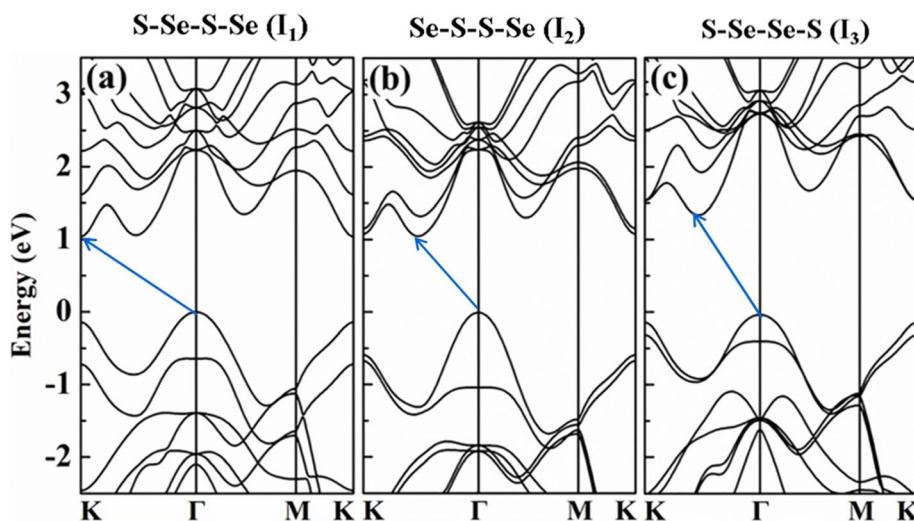

Fig. 3 Band structures of I_1, I_2, and I_3, respectively, where the bandgaps are denoted by the blue arrows
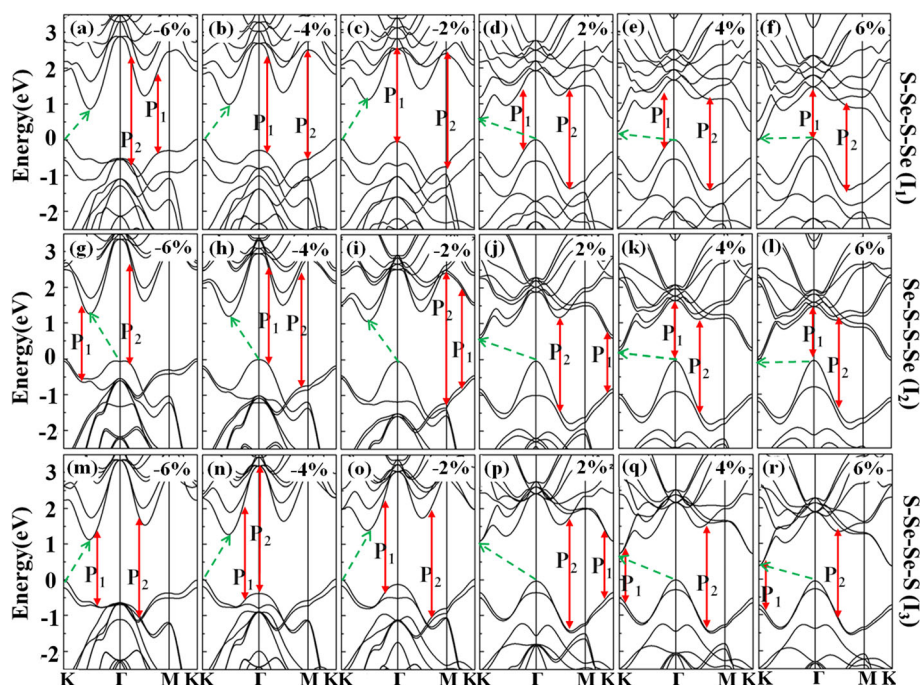
Fig. 4 a–r Band structures of I_1, I_2, and I_3 with different strains of − 6%, − 4%, − 2%, 2%, 4%, and 6%, respectively. The bandgaps are denoted with the dashed green arrows, while red solid arrows depict the principal interband transitions of P_1 and P_2, respectively

As shown in Fig. 2, for all the stacking structures, chalcogen layers with the order of S-Se-Se-S possess the largest binding energy, while the reversed order Se-S-S-Se has the smallest binding energy. In addition, it is visualized that AA', AA', and AB are the most stable stacking configurations of S-Se-Se-S, S-Se-S-Se, and Se-S-S-Se orders, with the binding energies of 0.322, 0.304, and 0.281 eV, respectively. This indicates that the Janus WSSe bilayer prefers to form a bilaterally symmetrical AA' stacking with the S-Se-Se-S chalcogen order, which is different from the MoSSe/WSSe heterostructure of AB stacking [33].
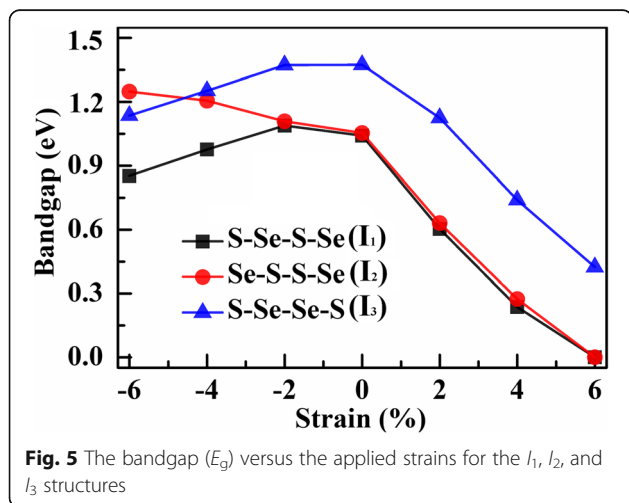

Fig. 5 The bandgap (E_g) versus the applied strains for the I_1, I_2, and I_3 structures

Considering the most stable stacking structures mentioned above for each chalcogen order, both the electronic and optical properties are profoundly investigated. For convenience, the AA' stacking with S-Se-S-Se structure, the AB stacking with Se-S-S-Se structure, and the AA' stacking with S-Se-Se-S structure are named as I_1, I_2, and I_3, respectively, in the following discussion.

Band structures of the Janus WSSe bilayers I_1, I_2, and I_3 are calculated, as shown in Fig. 3. All the three configurations exhibit a fundamental indirect bandgap structure, which is similar to that of the pure bilayer WS_2 and WSe_2. The valence band maximums (VBM) are all locating at Γ point, while the conduction band minimum (CBM) locating at K point for I_1, and situating between K and Γ points for both I_2 and I_3. The indirect bandgap of I_3 is calculated to be roughly 1.3 eV, slightly larger than that of I_1 and I_2 whose bandgaps are approximately 1.0 eV. Despite that the bandgaps are underestimated without the screened hybrid HSE06 functional, the band structure distributions have no significant change, and thus, the underestimation will not substantially influence the evolution tendency of the electronic properties under the strain modulation.

Strain engineering is a promising method for manipulating the structural symmetry and the interlayer interaction, which could give rise to plenteous charming phenomena. To study the electronic structures of WSSe bilayers modulated by the applied strain, the energy bands are analyzed, as illustrated in Fig. 4a–r. When a
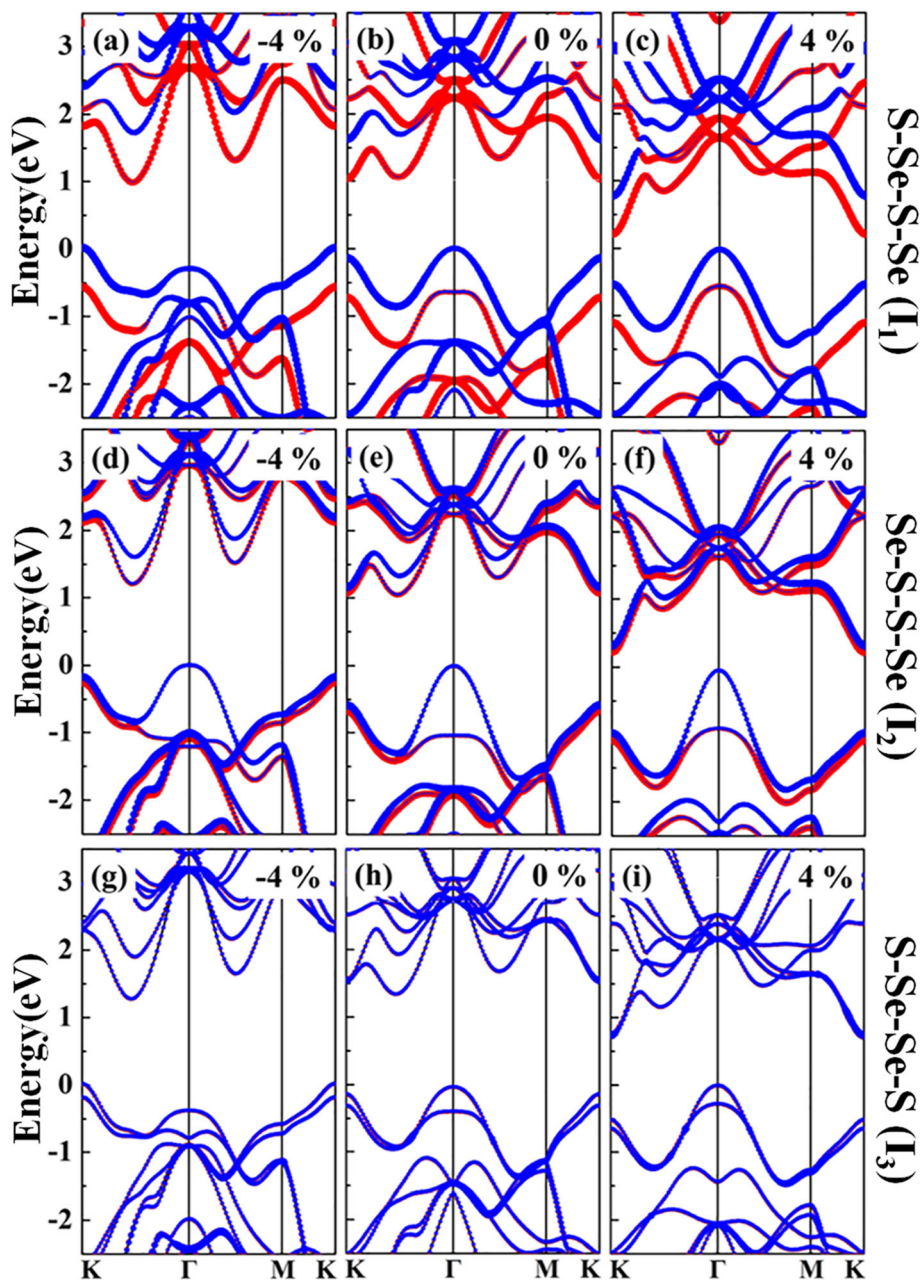
Fig. 6 Atomic orbital projected energy bands of I_1, I_2, and I_3 structures under the strains of − 4%, 0, and 4%, respectively. Blue and red colors mean orbital contributions from the upper and the lower layers, respectively

compressive strain ranging from − 6 to − 2% is applied, the original VBM at Γ point changed to K point for I_1 and I_3 configurations, while shows little variety for I_2. The original CBM at K point shifts to the position between Γ and K points for all the three structures. Once the tensile strain in the region of 2%~6% is employed, the VBM remains at Γ point while the CBM is all locating at the K point.

Figure 5 summarizes the strain-dependent bandgap for the three structures. It is apparent at a glance that the

responses of the bandgap to compressive strain and tensile strain are not only with inequal responsivity but also with different gradients as the applied strain increases. The bandgap is less sensitive to compressive strain, while dramatically decreases with the enhanced tensile strains. As the compressive strain increases, the CBM of both I_1 and I_3 is uplifted to higher energy, whereas that of I_2 is downshifted to lower energy, resulting in a slight decrease for I_2 and increase for I_1 and I_3 in the indirect bandgaps. In the presence of the tensile strain, the CBM
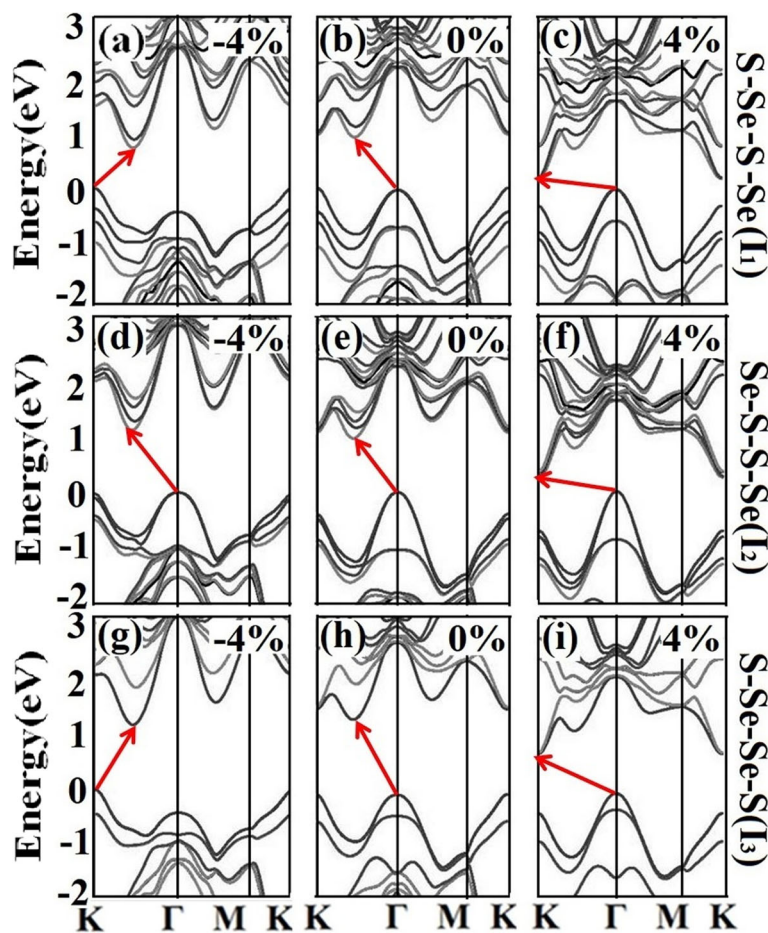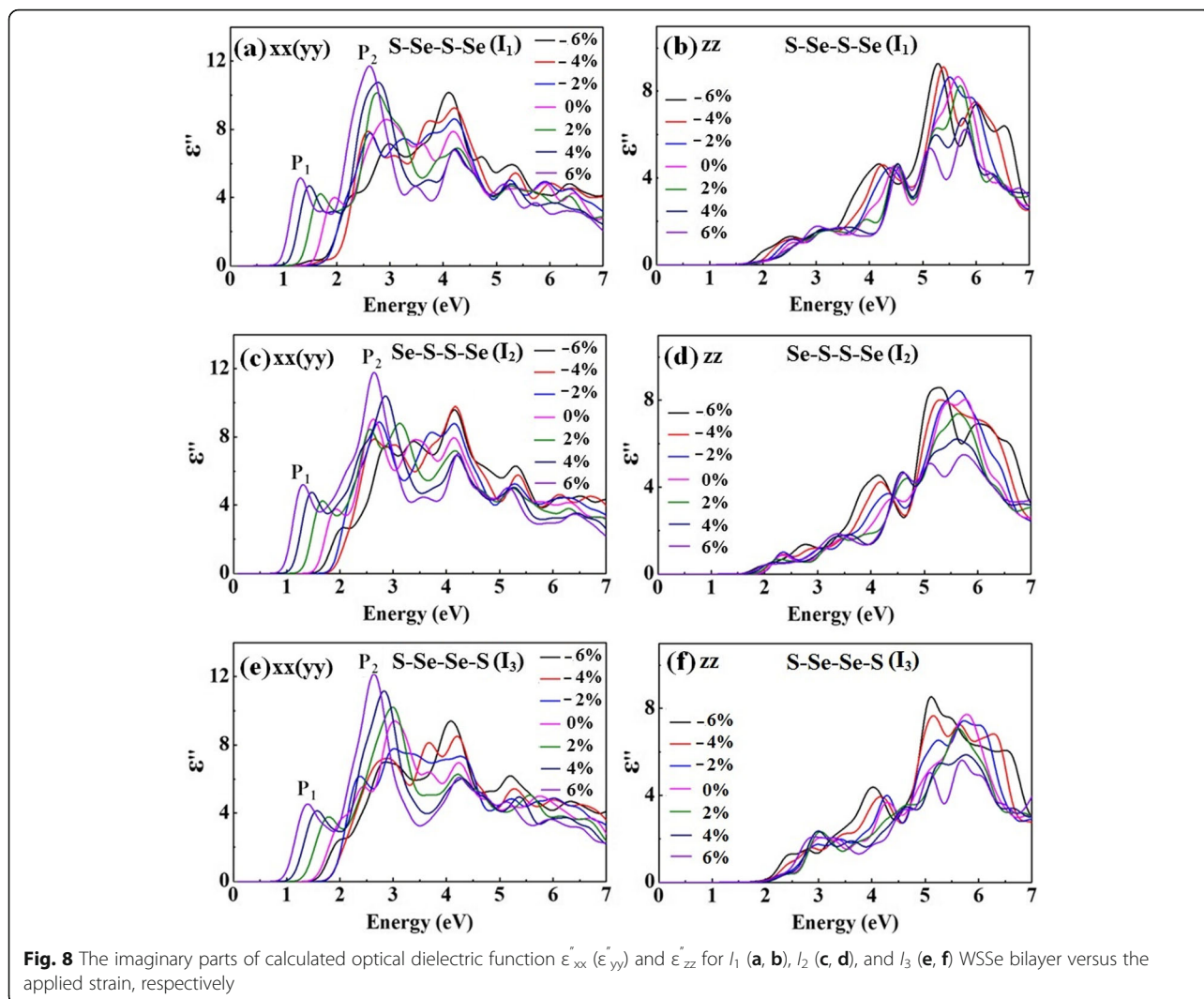
Fig. 7 a–i Band structures of I_1, I_2, and I_3 under the strains of − 4%, 0, and 4% with the consideration of SOC effect, where the black and blown colors mean the up and down spins, respectively. The bandgaps are denoted by the red arrows

enormously decreases while the VBM rises gently. The indirect bandgap thus exhibits a conspicuous diminishment and decreases sharply when the tensile strain reaches 6%. Compared with that of the strained Janus WSSe monolayer [34], the bandgaps of I$_1$ and I$_3$ show generally similar evolution with both compressive and tensile strain modulations, while the bandgap of I$_2$ behaves oppositely under the compressive strains.

In order to gain an insight into the electronic structure of WSSe bilayer in the presence of the strains, the atomic orbital projected energy band is studied, as seen in Fig. 6. Owing to its center inversion symmetry (Fig. 1l), the orbitals of the upper and lower layers for I_3 are energy degenerate, which make identical contributions to the band structure. On the contrary, because of the structure inversion asymmetry of I_1 and I_2, the orbitals of the upper and lower layers are splitted. The above results suggest that there is a positive correlation between the degeneracy and the structural symmetry. Owing to the center inversion symmetry of I_3 stacking, the orbitals of the upper and lower layers for I_3 are energy

degenerate, which make identical contributions to the band structure regardless of the varying strains. As depicted in Fig. 6g–i, both the CBM and VBM equally derived from the two WSSe layers. On the contrary, because of the structural inversion asymmetry of I_1 and I_2, the orbitals of the two layers are splitted, as shown in Fig. 6a–c and Fig. 6d–f. The original I_1 structure exhibits a typical type-II heterostructure, with the CBM and VBM contributed from the lower and upper WSSe Janus layers, respectively. The band alignment does not vary under either the compressive or tensile strains (Fig. 6a–c). As for the I_2 stacking without and with a compressive strain, the CBM comes from both the two layers, and the VBM originates from the upper layer (Fig. 6d, e). The I_2 heterostructure changes to a type-II band alignment under the tensile strain (Fig. 6f), which indicates a promising prospect for developing high-performance optoelectric conversion and energy storage devices [35].

To further explore the spin-orbit coupling (SOC) effect in the strain engineering in the WSSe bilayer, the band structures with the consideration of SOC are

Guo *et al. Nanoscale Research Letters* (2020) 15:97

Page 7 of 9

Fig. 8 The imaginary parts of calculated optical dielectric function ε''_{xx} (ε''_{yy}) and ε''_{zz} for I_1 (**a**, **b**), I_2 (**c**, **d**), and I_3 (**e**, **f**) WSSe bilayer versus the applied strain, respectively

further calculated without and with the strains of − 4% and 4%, as shown in Fig. 7. It is found that, for all the three configurations, the band structures including the momentum positions of VBM and CBM, the bandgaps, and band distributions show similar evolution tendency with the varying strains. This suggests that the strain modulation regularity still remains, and the SOC effect does not obviously influence the main conclusions.

With the aim to modulate the optical properties of the WSSe bilayer, the response of the dielectric function under external varying strain is studied. Figure 8 displays the complex dielectric function ε''_{xx} (ε''_{yy}) and ε''_{zz} of WSSe bilayer versus the applied strain. ε''_{xx} (ε''_{yy}) is found to shift to lower energies with the increasing tensile strain, and on the contrary, shift to the higher energy region while a compressive strain is applied. Compared with the unstrained WSSe bilayer with the dipole transition of 0.79, 1.18, and 1.15 eV, respectively for I_1, I_2, and I_3 structures, the strain modulation is able to obtain a

wide-range transition energy from 0.24 to 1.47 eV in near-infrared and mid-infrared area, which could be offering extensive possibilities for assorted detectors, for instance, infrared detector and pyroelectric detector.

The main peaks in the imaginary part of the dielectric function labeled as P_1 and P_2 in Fig. 8a, c, and e could be assigned to the principal interband transitions. This is achieved by fitting the peak energies in Fig. 8 with that of the interband transitions in Fig. 4. When a strain ranging from − 6 to 6% is applied, the peak energies of P_1 and P_2 increase firstly and then decrease. Regardless of the strains, both the P_1 and P_2 peaks are found to take place in the energy range of 1.3–3.0 eV, which exhibit great enhanced response in a wide spectrum from ultraviolet, visible to the near-infrared area. The widely distributed peaks should be suitable for the design of multiband metamaterial emitters with promising photoelectric applications.

Controllable anisotropy of WSSe bilayer through the strain engineering is further investigated. Compared with that of $\varepsilon^{''}_{xx}$ ($\varepsilon^{''}_{yy}$), $\varepsilon^{''}_{zz}$ exhibits insignificant variation regardless of the tensile or compressive strain. This manifests the fact that the imaginary part of the dielectric function possesses different response properties with the increased strain. Without the strain, the $\varepsilon^{''}_{xx}$ ($\varepsilon^{''}_{yy}$) and $\varepsilon^{''}_{zz}$ are anisotropy with E∥ĉ transformation preference for all the I_1, I_2, and I_3 structures. For either I_1 or I_3, while a compressive strain is applied, the anisotropy of dipole transition is firstly enhanced and then weakened and that with the tensile strain is always enhanced. Nevertheless, the anisotropy of I_2 is enhanced with the increasing tensile strain and becomes weakened once a compressive strain is introduced. An isotropy of dipole transition occurs when the compressive strain continues to increase to − 6%~− 4%, where both E∥ĉ and E⊥ĉ possess equal transformation preference. Thus, the WSSe bilayer with a suitable strain modulation will be leading to a transition from optical anisotropy to isotropy. Since the excitonic effect usually plays an important role in the optical absorption [36, 37], the dielectric function determined dipole transition preference may be explored for the potential optoelectronic applications with an electroluminescence process.

As has been demonstrated that some typical TMDC monolayers with 2H phase have the same hexagonal lattices and similar characters in their monolayer band structures [5, 33, 38, 39]. Therefore, the Janus monolayer and bilayer derived from these TMDC materials, such as MXY (M = Mo or W, X/Y = S, Se, or Te, and $X \neq Y$), would be expected to possess similar band structures [8, 32] and thus the similar electronic and optical properties, as well as evolution tendency with strain modulation. Therefore, the main calculation results will have certain universality in 2H-TMDC Janus materials. Going through the previous reports, the mechanical properties of out-of-plane bended MoS_2 thin films have been revealed [40], the electronic and optical properties of TMDC compounds have been studied [22], and the energy gaps of monolayer and Janus heterobilayer TMDCs have been demonstrated to control the electric field [41]. Comparing with these works, we provide a series of innovative results in strain-modulated electronic and optical properties of 2D Janus WSSe bilayer, which enriches the physical connotation of the Janus materials and provides a promising control strategy towards the application of next-generation electronic and optoelectronic nanodevices.

Conclusion

In summary, the strain dependence of electronic and optical properties of the WSSe bilayer is systematically studied. By comparing the binding energies of different stackings, the most favorable configuration of the WSSe bilayer is determined. The WSSe bilayer preserves an indirect bandgap structure, which is sensitive to the external stress. The bandgap of all the stable structures can be tailored from the semiconductor to metallicity under to obtain a wide-range spectrum in near-infrared and mid-infrared area. Atomic orbital projected energy bands reveal a positive correlation between the degeneracy and the structural symmetry, which explains the bandgap evolutions. Dipole transition preference is investigated from the dielectric properties and tuned by the biaxial strain. Under around − 6%~− 4% critical strain, a controllable transformation between anisotropic and isotropic optical properties is realized. The strain-modulated electronic and optical behaviors of Janus WSSe bilayer possess a wide application prospect in next-generation electronic and optoelectronic nanodevices.

References
1. Sarkar D, Xie X, Liu W, Cao W, Kang J, Gong Y, Kraemer S, Ajayan P, Banerjee K (2015) A subthermionic tunnel field-effect transistor with an atomically thin channel. Nature. 526:91–95
2. Withers F, Del Pozo-Zamudio O, Mishchenko A, Rooney A, Gholinia A, Watanabe K, Taniguchi T, Haigh S, Geim A, Tartakovskii A, Novoselov K (2015) Light-emitting diodes by band-structure engineering in van der Waals heterostructures. Nat Mater 14:301–306
3. Plechinger G, Korn T, Lupton J (2017) Valley-polarized exciton dynamics in exfoliated monolayer WSe_2. J Phys Chem C 121:6409–6413
4. He P, Brent J, Ding H, Yang J, Lewis D, O'Brien P, Derby B (2018) Fully printed high performance humidity sensors based on two-dimensional materials. Nanoscale. 10:5599–5606

5. Cheng Y, Zhu Z, Tahir M, Schwingenschlögl U (2013) Spin-orbit-induced spin splittings in polar transition metal dichalcogenide monolayers. EPL. 102:57001
6. Er D, Ye H, Frey N, Kumar H, Lou J, Shenoy V (2018) Prediction of enhanced catalytic activity for hydrogen evolution reaction in Janus transition metal dichalcogenides. Nano Lett 18:3943–3949
7. Karande S, Kaushik N, Narang D, Late D, Lodha S (2016) Thickness tunable transport in alloyed WSSe field effect transistors. Appl Phys Lett 109:142101
8. Zhou W, Chen J, Yang Z, Liu J, Ouyang F (2019) Geometry and electronic structure of monolayer, bilayer, and multilayer Janus WSSe. Phys Rev B 99: 075160
9. Zhang F, Zhang H, Krylyuk S, Milligan C, Zhu Y, Zemlyanov D, Bendersky L, Burton B, Appenzeller A (2019) Electric-field induced structural transition in vertical MoTe$_2$ and Mo$_{1-x}$WxTe$_2$ based resistive memories. Nat Mater 18: 55–61
10. Ke C, Wu Y, Guo G, Lin W, Wu Z, Zhou C, Kang J (2018) Tuning the electronic, optical, and magnetic properties of monolayer GaSe with a vertical electric field. Phys Rev Appl 9:044029
11. Kansara S, Gupta K, Sonvane K (2018) Effect of strain engineering on 2D dichalcogenides transition metal A DFT study. Comput Mater Sci 141:235–242
12. Li X, Zhang S, Wang Q (2017) Topological insulating states in 2D transition metal dichalcogenides induced by defects and strain. Nanoscale. 9:562–569
13. Jiang J, Ni Z (2019) Defect engineering in two-dimensional materials. J Semicond 40:070403
14. Rafiq M (2018) Carrier transport mechanisms in semiconductor nanostructures and devices. J Semicond 39:061002
15. Liu B, Wu L, Zhao Y, Wang L, Cai M (2016) A first-principle study of magnetic variation via doping vacancy in monolayer VS$_2$. J Magn Magn Mater 420:218–224
16. Liu J, Hou CC, Fu H, Sun J, Meng S (2017) Intrinsic valley polarization of magnetic VSe$_2$ monolayers. J Phys Condens Matter 29:255501
17. Luo N, Si C, Duan W (2017) Structural and electronic phase transitions in ferromagnetic monolayer VS$_2$ induced by charge doping. Phys Rev B 95: 205432
18. Peng G, Lo P, Li W, Huang Y, Chen Y, Lee C, Yang C, Cheng S (2019) Distinctive signatures of the spin- and momentum-forbidden dark exciton states in the photoluminescence of strained WSe$_2$ monolayers under thermalization. Nano Lett 19:2299–2312
19. Gujarathi D, Solanki G, Deshpande M, Agarwal M (2005) Band gap in tungsten sulphoselenide single crystals determined by the optical absorption method. Mater Sci Semicond Process 8:576–586
20. Ni Z, Yu T, Lu Y, Wang Y, Feng Y, Shen Z (2008) Uniaxial strain on graphene: raman spectroscopy study and band-gap opening. ACS Nano 2:2301–2305
21. McCann E (2006) Asymmetry gap in the electronic band structure of bilayer graphene. Phys Rev B 74:161403
22. Rafael R, Silva-Guillén J, López-Sancho M, Guinea F, Cappelluti E, Ordejón P (2014) Electronic properties of single-layer and multilayer transition metal dichalcogenides MX$_2$(M= Mo, W and X= S, Se). Ann Phys (Berlin) 526:347–357
23. Li L, Carter P (2019) Defect-mediated charge-carrier trapping and nonradiative recombination in WSe$_2$ monolayers. J Am Chem Soc 141: 10451–10461
24. Yang Q, Yuan R, Guo Y (2019) Valley switch effect based on monolayer WSe$_2$ modulated by circularly polarized light and valley Zeeman field. J Phys D Appl Phys 52:335301
25. Yea L, Wang P, Luo W, Gong F, Liao L, Liu T, Tonga L, Zang J, Xu J, Hu W (2017) Highly polarization sensitive infrared photodetector based on black phosphorus-on-WSe$_2$ photogate vertical heterostructure. Nano Energy 37: 53–60
26. Rehman J, Roshan A, Nisar A, Lv X, Guo C (2019) Theoretical investigation of strain-engineered WSe$_2$ monolayers as anode material for Li-ion batteries. J Alloys Compd 804:370–375
27. Kresse G, Hafner J (1994) Ab initio molecular-dynamics simulation of the liquid-metal-amorphous-semiconductor transition in germanium. Phys Rev B 49:14251
28. Kresse G, Furthmüller J (1996) Efficient iterative schemes for ab initio total-energy calculations using a plane-wave basis set. Phys Rev B 54:11169
29. Kresse G, Joubert D (1999) From ultrasoft pseudopotentials to the projector augmented-wave method. Phys Rev B 59:1758
30. Kim Y, Hummer K, Kresse G (2009) Accurate band structures and effective masses for InP, InAs, and InSb using hybrid functionals. Phys Rev B 80: 035203
31. Perdew J, Burke K, Ernzerhof M (1996) Generalized gradient approximation made simple. Phys Rev Lett 77:3865
32. Kandemir A, Sahin H (2018) Bilayers of Janus WSSe: monitoring the stacking type via the vibrational spectrum. Phys Chem Chem Phys 25(20):17380–17386
33. Li F, Wei W, Zhao P, Huang B, Dai Y (2017) Electronic and optical properties of pristine and vertical and lateral heterostructures of Janus MoSSe and WSSe. J Phys Chem Lett 8:5959–5965
34. Chaurasiya R, Dixit A, Pandey R (2018) Strain-mediated stability and electronic properties of WS$_2$, Janus WSSe and WSe$_2$ monolayers. Superlattice Microst 122:268–279
35. Ke C, Tang W, Zhou J, Wu Z, Li X, Zhang C, Wu Y, Yang W, Kang J (2019) Stress engineering on the electronic and spintronic properties for a GaSe/HfSe$_2$ van der Waals heterostructure. Appl Phys Express 12:031002
36. Kuklin A, Ågren H (2019) Quasiparticle electronic structure and optical spectra of single-layer and bilayer PdSe$_2$: proximity and defect-induced band gap renormalization. Phys Rev B 99:245114
37. Shi H, Pan H, Zhang Y, Yakobson B (2013) Quasiparticle band structures and optical properties of strained monolayer MoS$_2$ and WS$_2$. Phys Rev B 87: 155304
38. Zhang Y, Ye H, Yu Z, Liu Y, Li Y (2019) First-principle study of square phase MX$_2$ and Janus MXY (M=Mo, W; X, Y=S, Se, Te) transition metal dichalcogenide monolayers under biaxial strain. Phys E 110:134–139
39. Guo S, Dong J (2018) Biaxial strain tuned electronic structures and power factor in Janus transition metal dichalchogenide monolayers. Semicond Sci Technol 33:085003
40. Zhu Y, Wang P, Xiao S, He S, Chen J, Jiang Y, Wang Y, He J, Gao Y (2018) Manipulating three-dimensional bending to extraordinarily stiffen two-dimensional membranes by interference colors. Nanoscale. 10:21782–21789
41. Liu Z, Lin Y, Cao C, Zou S, Xiao J, Jin X, Chen L (2018) First-principle study of electronic and sodium-ion transport properties of transition-metal dichalcogenides. Int J Mod Phys B 32:1850215

Publisher's Note